

Weak Chaos and Fractional Dynamics in an Optically Driven Colloidal Ring

Yael Roichman and David G. Grier

Department of Physics and Center for Soft Matter Research, New York University, New York, NY 10003

George Zaslavsky

Department of Physics and Courant Institute, New York University, New York, NY 10003

(Dated: September 3, 2018)

Three colloidal spheres driven around a ring-like optical trap known as an optical vortex have been predicted to undergo periodic collective motion due to their hydrodynamic coupling. In fact, the quenched disorder in the optically-implemented potential energy landscape drives a transition to instability evolving into microscopic weak chaos with fractional dynamics. As a result, the relation between the space-time selfsimilarity of the system's collective transport properties and its microscopic weak chaos dynamics is revealed.

Three identical spheres slowly sedimenting through a viscous fluid in two or three dimensions generically tumble chaotically [1]. When the particles are driven steadily around a ring, by contrast, their motion is predicted to be purely periodic [2], with the reduction in dimensionality and the imposition of periodic boundary conditions [3] effectively eliminating the domain of chaotic dynamics. In this Letter, we demonstrate experimentally that chaos can be restored to this system by imposing a small amount of quenched periodic disorder. The hydrodynamically coupled spheres' collective motions, furthermore, are characterized by fractional dynamics.

Our system consists of colloidal silica spheres $1.58\ \mu\text{m}$ in diameter (Bangs Laboratories, Inc. PS04N) dispersed in a layer of water $40\ \mu\text{m}$ thick between a glass microscope slide and a coverslip. Three of these spheres are confined to a horizontal ring $12\ \mu\text{m}$ in diameter by a single-beam optical trap known as an optical vortex [4, 5, 6]. An optical vortex is formed by bringing a helical mode of light [7] to a focus with a high-numerical-aperture lens. The helical mode's wavefronts form an ℓ -fold helix, where ℓ is an integer winding number known as the topological charge. The axial ℓ -fold screw dislocation results in perfect destructive interference along the optical axis, so that the beam focuses to a ring of light whose radius is proportional to ℓ [8, 9]. Polarizable particles are drawn up intensity gradients to the bright ring, where they are trapped. Each photon in a helical beam, moreover, carries $\ell\hbar$ orbital angular momentum that can be transferred to trapped objects [10]. This creates a constant torque that drives the particles around the ring.

Our samples are mounted on the stage of a Nikon TE-2000U inverted optical microscope, whose objective lens ($100\times$ NA 1.4 oil immersion Plan-Apo) is used both to project an optical vortex and also to create images of trapped objects. We imprint helical phase profiles onto the wavefronts of a TEM₀₀ beam (Coherent Verdi, $\lambda = 532\ \text{nm}$) using a phase-only spatial light modulator (Hamamatsu X6750 PPM) in the holographic optical trapping configuration [11, 12, 13].

Figure 1(a) shows an optical vortex with $\ell = 80$ whose

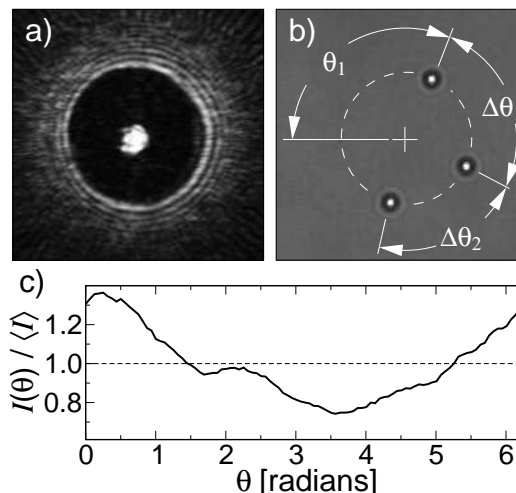


FIG. 1: Optically driven colloidal ring. (a) Projected intensity pattern for an optical vortex with $\ell = 80$. (b) Video microscope image of three colloidal silica spheres trapped on the optical vortex. (c) Measured intensity variations around the optical vortex's circumference.

image was obtained by placing a front-surface mirror in the microscope's focal plane and collecting the reflected light with the objective lens. The bright central spot is a conventional optical tweezer formed on the optical axis by the undiffracted portion of the laser beam. After adaptively correcting for residual aberrations in the optical train [13, 14], the optical vortex is a nearly uniform ring of light with radius $R_\ell = 12\ \mu\text{m}$. Figure 1(b) shows three colloidal spheres trapped on the ring at 2.5 W. Under these conditions, the particles circulate once around the ring in $T = 1.2\ \text{s}$. We track the spheres' angular positions, $\theta_1(t)$, $\theta_2(t)$ and $\theta_3(t)$, by recording the video stream at 30 frames per second to a Pioneer 520H-S digital video recorder (DVR) with a NEC TI-324AII monochrome video camera and extracting their instantaneous positions at 20 nm resolution using standard methods of digital video microscopy [15].

The optical vortex's peak intensity, plotted in Fig. 1(c)

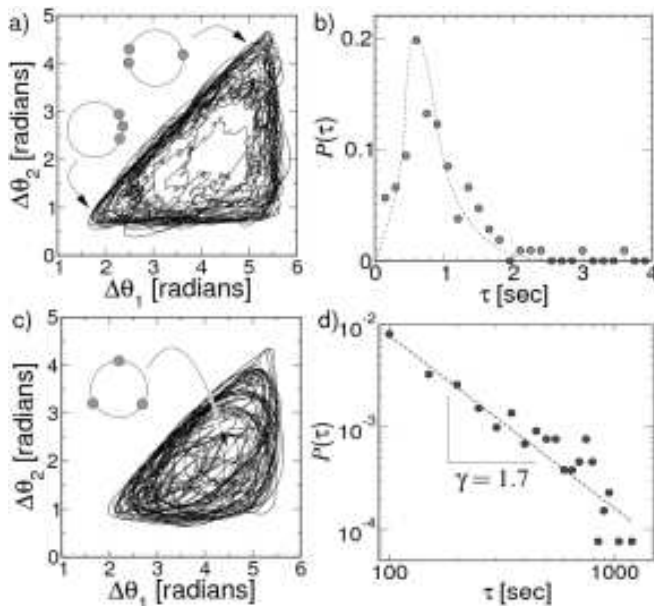


FIG. 2: (a) Projection of the phase space reconstructed from particle tracks at $\ell = 50$. (b) Recurrence time distribution for $\ell = 50$. The curve is a guide to the eye suggesting a cycle period of 0.6 s (c) Phase space at $\ell = 80$. (d) Recurrence time distribution for $\ell = 80$.

varies by about 20 percent from the mean around its circumference. These intensity variations establish an effective potential energy landscape for the circulating particles resulting from variations in the local orbital angular momentum flux and from optical gradient forces [16]. None of these variations is severe enough to trap a particle, and speed fluctuations for a single fluctuating particle suggest that relative mean-square variations in the effective potential are smaller than 5 percent [16, 17, 18]. Structure in the potential energy landscape is fixed in both position and time and therefore contributes quenched disorder to the particles' dynamics.

A circulating sphere entrains flows in the surrounding fluid that exert forces on the neighboring spheres. Treating the hydrodynamic coupling in the stokeslet approximation [19] reveals that the most symmetric state, with the particles equally spaced around the ring, is linearly unstable against a dynamical state in which two closely spaced spheres outrun the third [2]. This periodic dynamical state ought to be observed almost exclusively. In practice, however, the experimental system can spend much of its time in the nominally unstable state.

We characterized the system's dynamics by reconstructing its phase space from measurements of the independent angular separations, $\Delta\theta_1(t) = \theta_2(t) - \theta_1(t)$ and $\Delta\theta_2(t) = \theta_3(t) - \theta_2(t)$, and their associated momenta. The results in Fig. 2(a) show one continuous trajectory obtained over 2.5 hours, and smoothed by box-car averaging over ten mean circulation periods, T . Smoothing

suppresses detailed structure in the phase space trajectory due to diffusion and disorder, and thus provides a clearer picture of the system's intrinsic behavior.

Figure 2(a) shows results from an optical vortex with $\ell = 50$ and $R_\ell = 8 \mu\text{m}$ that reveal the predicted periodic orbit [2]. The parametric trace resembles a torus, with a pair of spheres racing around the ring to catch up to the remaining isolated sphere to form a transient three-particle cluster, whose leading pair then leaves the remaining sphere behind. The characteristic cycle time of $\tau = 0.6$ s substantially exceeds the 0.3 s required for an individual particle to circulate once around the ring.

Increasing the topological charge to $\ell = 80$ increases optical vortex's radius and reduces its mean intensity proportionately. Both the increased interparticle separation and the decreased mean circulation rate weaken the interparticle hydrodynamic coupling. The quenched disorder is proportional to the local intensity, and thus is comparatively stronger in the larger optical vortex. Under these circumstances, the particles' trajectories, plotted in Fig. 2(c), make frequent and extended excursions away from the nominally stable period cycle into the region of phase space corresponding to the nominally unstable equilateral configuration.

We characterized this model system's microscopic dynamics by measuring the distribution of recurrence times, τ required for a trajectory to revisit regions of phase space $\delta\theta = 0.5$ rad on a side. The results for $\ell = 50$ are plotted in Fig. 2(b) and are consistent with a simple cycle with a period of 0.7 s. Those for $\ell = 80$, plotted in Fig. 2(d), display no periodicity, nor are they consistent with the exponential distribution that would be expected for fully developed chaos. Instead, they follow a power-law decay, with an exponent $\gamma = 1.7 \pm 0.1$.

Power-law divergence of trajectories in phase space is a defining characteristic of weak chaos [20]. Its emergence in periodically kicked overdamped dynamical systems has been inferred from measurements on nonlinear Alfvén waves in plasmas [21, 22] and in low-dimensional wall flow of viscous fluids [23]. Unlike these pioneering studies, we have direct experimental access to the relevant microscopic degrees of freedom, and therefore do not have to reconstruct the phase space structure from measurements of collective properties.

Quenched periodic disorder is known to induce transitions to chaos in a wide variety of Hamiltonian and non-Hamiltonian systems. The appearance of weak chaos in a strongly overdamped system is far less common. Other overdamped systems displaying noise-induced chaos [24] rely on thermal forces to fully explore phase space. The optically-driven colloidal ring, by contrast, is athermal.

Particles circulating around an optical vortex are affected by three factors: the spheres' hydrodynamic interactions, the periodic potential landscape, and Brownian motion. The importance of each can be inferred by comparing the measured [15] free-particle self-diffusion coefficient

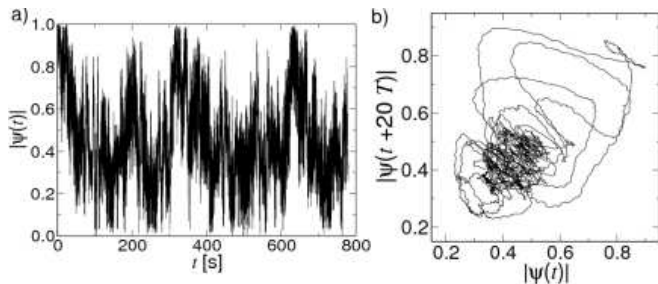


FIG. 3: (a) Evolution of the three-fold bond-orientational order parameter. (b) Phase space reconstructed from $\psi(t)$.

cient $D_0 = 0.19 \pm 0.02 \mu\text{m}^2/\text{s}$ with that of a single sphere in an optical vortex [16], $D_1 = 1.0 \pm 0.2 \mu\text{m}^2/\text{s}$, and with that of one of the three spheres in the complete system, $D_3 = 2.0 \pm 0.3 \mu\text{m}^2/\text{s}$. The individual sphere's effective diffusivity exceeds the free-particle value by a factor of five, demonstrating that the landscape's quenched disorder has far more influence than thermal forces. The fluctuations, moreover, have a non-Gaussian distribution that reflects the intensity variations around the optical vortex, rather than thermal forcing. This differs from giant amplification of thermal fluctuations that can occur when particles become marginally trapped in local potential energy wells [16, 25]. That fluctuations increase by another factor of two with three particles on the same ring demonstrates that hydrodynamic coupling is stronger still. Because hydrodynamic coupling alone would yield a periodic orbit [2], the weakly chaotic dynamics we observe must be due to the quenched disorder. Thermal fluctuations do not contribute appreciably to the microscopic dynamics of the observable three-particle system, at least in this range of parameters.

It has long been known that periodic perturbations can induce chaos in dissipative systems possessing a stable limit cycle [26]. Here, hydrodynamic coupling is responsible for the limit cycle [2] and the combination of viscous damping and quenched disorder causes the system to sample other parts of phase space. Not any landscape will do this, however. As suggested in [26] and proved in [27, 28], a periodic perturbation can open up a chaotic attractor near a stable limit cycle if the perturbation possesses a fairly broad frequency spectrum, for instance if it consists of sharp kicks. The potential energy landscape inferred from Fig. 1(c) has this property, kicking the three-particle system three times during each cycle.

Having direct access to a chaotic system's microscopic degrees of freedom presents a rare opportunity to track how weak chaos in the microscopic dynamics of an experimental system influences macroscopic properties. To show this, we combine the three trajectories into the com-

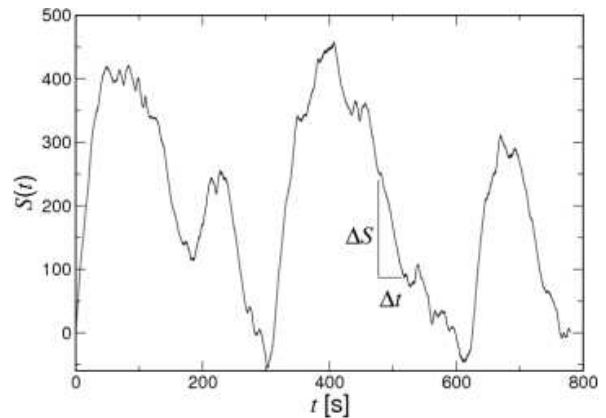


FIG. 4: Running sum, $S(t)$, of the three-fold bond-orientational order parameter, displaying a hierarchy of jumps ΔS spanning a range of durations Δt .

plex three-fold bond-orientational order parameter,

$$\psi(t) = \frac{1}{3} \sum_{j=1}^3 \exp(3i\theta_j(t)), \quad (1)$$

where θ_j is measured with respect to a fixed reference direction. This function's phase tracks the system's rotation about the optical axis and is useful for measuring the mean cycle period T . Its magnitude, $|\psi(t)|$, reaches unity when the spheres are evenly spaced and drops to roughly one third when a pair of spheres is diametrically opposite from the third.

The trace of $|\psi(t)|$ in Fig. 3(a) is computed for the trajectory data in Fig. 2(c) and provides a macroscopic overview of the system's microscopic dynamics, akin to observing the Brownian motion of a colloidal sphere as a probe of the microscopic dynamics of the surrounding fluid. As for other effective macroscopic descriptors, $\psi(t)$ can be used to reconstruct the underlying microscopic phase space. For example, Fig. 2(b) shows a Poincare section at delay $20T$, which effectively fills the accessible part of the phase space. The periodic state concentrates the trajectory around $(1/3, 1/3)$, while occasional excursions to the equilateral state fill out the pattern.

The order parameter's magnitude also reveals that the system switches intermittently between paired and equilateral states. To analyze the intermittent dynamics we use methods originally developed to interpret density fluctuation data obtained from tokamak plasmas [29]. Given measurements of $\psi(t)$ at N discrete times t_k , the running sum

$$S(t_n) = \sum_{k=1}^n |\psi(t_k)| - \frac{n}{N} (|\psi(t_N)| - |\psi(t_1)|) \quad (2)$$

minimizes the noise in $|\psi(t)|$ and emphasizes jumps at different scales, as shown in Fig. 4. Jumps in $S(t)$ may

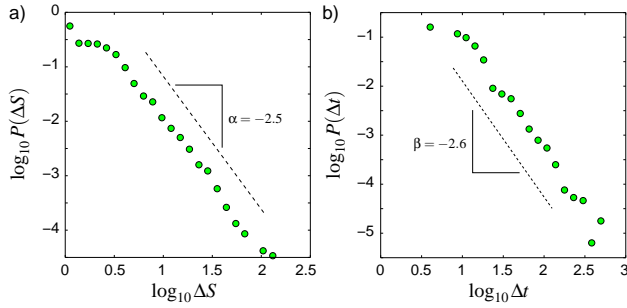


FIG. 5: Scaling of the magnitude and duration distributions for jumps in $S(t)$.

be identified as flights in a system with fractional dynamics. One then can consider the distribution functions, $P_S(\Delta S)$ and $P_t(\Delta t)$, for the magnitudes, ΔS , and durations Δt of these flights. The corresponding results are presented in Fig. 5.

Not only does $|\psi(t)|$ display intermittent jumps, but its two-state structure appears also to be scale-invariant. Both the probability distribution for jump magnitudes and jump durations are well described by power laws. The exponents $\alpha = -2.5 \pm 0.1$ and $\beta = -2.6 \pm 0.2$ for the magnitude and duration distributions, respectively, are consistent with each other, and both exceed 2. This is a signature of fractional kinetics in the system's chaotic collective dynamics [20].

Equality of α and β arises naturally in any system undergoing ballistic flights. For the three colloidal spheres in the present model system, these flights take the form of random transitions between the equilateral and periodic dynamical states. Furthermore, log-periodic oscillations are evident when $S(t)$ is plotted on a logarithmic time scale. Such log-periodicity arises for processes characterized by discrete scaling [20, 30] and can be considered as evidence for hierarchical structure in the system's collective dynamics. The resulting self-similar structure of weakly chaotic dynamics is predicted [20] to yield a relationship between the scaling in the distribution of microscopic recurrence times and the distribution of macroscopic flight durations, $P(\tau) d\tau = P_t(\Delta t) d\Delta t$. This leads to the prediction $\gamma = \alpha - 1$, which is consistent with our experimental results.

We have demonstrated that imposing a small amount of quenched disorder on an optically driven colloidal ring can induce a transition from a periodic steady state to weakly chaotic dynamics characterized by fractional time-space scaling. Because the circulating particles in our experiments repeatedly sample the same fixed optical intensity pattern, this disorder results in periodic driving with strong kicks. Consequently, this provides a model system for studying disorder-induced transitions to chaos in which both the microscopic and macroscopic degrees of freedom are experimentally accessible.

This work was supported by the National Science

Foundation through Grant Number DMR-0451589. G.Z. was supported by the ONR Grant N00014-02-1-0056. We would like to thank Pablo Jercog for inspiring discussions and M. Edelman for the help in preparing Fig. 5.

-
- [1] I. M. Jánosi, T. Tél, D. E. Wolf, and J. A. C. Gallas, Phys. Rev. E **56**, 2858 (1997).
 - [2] M. Reichert and H. Stark, **16**, S4085 (2004).
 - [3] M. L. Ekiel-Jezewska and B. U. Felderhof, Physics of Fluids **17**, 093102 (2005).
 - [4] H. He, N. R. Heckenberg, and H. Rubinsztein-Dunlop, J. Mod. Opt. **42**, 217 (1995).
 - [5] K. T. Gahagan and G. A. Swartzlander, Opt. Lett. **21**, 827 (1996).
 - [6] N. B. Simpson, L. Allen, and M. J. Padgett, J. Mod. Opt. **43**, 2485 (1996).
 - [7] L. Allen, M. W. Beijersbergen, R. J. C. Spreeuw, and J. P. Woerdman, Phys. Rev. A **45**, 8185 (1992).
 - [8] J. E. Curtis and D. G. Grier, Phys. Rev. Lett. **90**, 133901 (2003).
 - [9] S. Sundbeck, I. Gruzberg, and D. G. Grier, Opt. Lett. **30**, 477 (2005).
 - [10] H. He, M. E. J. Friese, N. R. Heckenberg, and H. Rubinsztein-Dunlop, Phys. Rev. Lett. **75**, 826 (1995).
 - [11] E. R. Dufresne and D. G. Grier, Rev. Sci. Instr. **69**, 1974 (1998).
 - [12] J. E. Curtis, B. A. Koss, and D. G. Grier, Opt. Comm. **207**, 169 (2002).
 - [13] M. Polin, K. Ladavac, S.-H. Lee, Y. Roichman, and D. G. Grier, Opt. Express **13**, 5831 (2005).
 - [14] Y. Roichman, A. S. Waldron, E. Gardel, and D. G. Grier, Appl. Opt. p. in press (2005).
 - [15] J. C. Crocker and D. G. Grier, J. Colloid Interface Sci. **179**, 298 (1996).
 - [16] S.-H. Lee and D. G. Grier, Phys. Rev. Lett. **96**, 190601 (2006).
 - [17] K. Ladavac, K. Kasza, and D. G. Grier, Phys. Rev. E **70**, 010901(R) (2004).
 - [18] M. Pelton, K. Ladavac, and D. G. Grier, Phys. Rev. E **70**, 031108 (2004).
 - [19] C. Pozrikidis, *Boundary Integral and Singularity Methods for Linearized Viscous Flow* (Cambridge University Press, New York, 1992).
 - [20] G. M. Zaslavsky and M. Edelman, Phys. Rev. E **72**, 036204 (2005).
 - [21] E. L. Rempel, A. C. L. Chian, A. J. Preto, and S. Stephany, Nonlinear Processes in Geophysics **11**, 691 (2004).
 - [22] L. F. Burlaga and A. F. Vinas, Physica A **356**, 375 (2005).
 - [23] J. Jimenez and M. P. Simens, J. Fluid Mech. **435**, 81 (2001).
 - [24] J. P. Crutchfield and B. A. Huberman, Phys. Lett. A **77**, 407 (1980).
 - [25] P. Reimann, C. Van den Broeck, H. Linke, P. Hänggi, J. M. Rubi, and A. Pérez-Madrid, Phys. Rev. Lett. **87**, 010602 (2001).
 - [26] G. M. Zaslavsky, Phys. Lett. A **69**, 145 (1978).
 - [27] Q. D. Wang and L. S. Young, Commun. Math. Phys. **218**, 1 (2001).

- [28] Q. D. Wang and L. S. Young, Commun. Math. Phys. **225**, 275 (2002). 3691 (2000).
- [29] G. M. Zaslavsky, M. Edelman, H. Weitzner, B. Carreras, G. McKee, R. Bravenec, and R. Fonck, Phys. Plasmas **7**, 3691 (2000).
- [30] D. Sornette, Physica A **250**, 295 (1998).